Magnetization and ^{13}C NMR spin-lattice relaxation of nanodiamond powder

E. M. Levin,[1,2,*] X. W. Fang,[3] S. L. Bud'ko,[1,2] W. E. Straszheim,[4] R. W. McCallum,[1,5] and K. Schmidt-Rohr[1,3,*]
[1]*Ames Laboratory DOE, Iowa State University, Ames, Iowa 50011, USA*
[2]*Department of Physics and Astronomy, Iowa State University, Ames, Iowa 50011, USA*
[3]*Department of Chemistry, Iowa State University, Ames, Iowa 50011, USA*
[4]*Materials Analysis and Research Laboratory, Iowa State University, Ames, Iowa 50011, USA*
[5]*Department of Materials Science and Engineering, Iowa State University, Ames, Iowa 50011, USA*
(Received 3 August 2007; revised manuscript received 19 November 2007; published 15 February 2008)

The bulk magnetization at temperatures of 1.8–400 K and in magnetic fields up to 70 kOe, the ambient temperature ^{13}C NMR spin-lattice relaxation, $T_{1,C}$, and the elemental composition of three nanodiamond powder samples have been studied. The total magnetization of nanodiamond can be explained in terms of contributions from (1) the diamagnetic effect of carbon, (2) the paramagnetic effect of unpaired electrons present in nanodiamond grains, and (3) ferromagneticlike and (4) superparamagnetic contributions from Fe-containing particles detected in spatially resolved energy-dispersive spectroscopy. Contributions (1) and (2) are intrinsic to nanodiamond, while contributions (3) and (4) arise from impurities naturally present in detonation nanodiamond samples. ^{13}C NMR $T_{1,C}$ relaxation would be unaffected by the presence of the ferromagnetic particles with the bulk magnetization of ~0.01 emu/g at 300 K. Thus, a reduction of $T_{1,C}$ by 3 orders of magnitude compared to natural and synthetic microdiamonds confirms the presence of unpaired electrons in the nanodiamond grains. The spin concentration in nanodiamond powder corresponds to ~30 unpaired electrons per ~4.6 nm diameter nanodiamond grain.

DOI: 10.1103/PhysRevB.77.054418 PACS number(s): 75.50.Tt, 75.20.−g, 76.60.−k

I. INTRODUCTION

Magnetism of all-carbon nanostructured materials is a subject of great interest because it is assigned to unpaired electron spins present in a diamagnetic matrix without any *d*-or *f*-paramagnetic ions. Major questions concern the origin of the unpaired electron spins resulting in paramagnetism of various materials and of exchange interactions between them, which may give rise to ferromagnetic order.

Contributions to the bulk magnetization of diamond, which is one of well known carbon allotropic modifications, have been discussed in detail by Hudgens *et al.*[1] and Heremans *et al.*[2] They showed that the magnetic susceptibility of carbon can be described by three terms: two Langevin-like diamagnetic terms from core and valence electrons, and a Van Vleck paramagnetic term from virtual magnetic dipole transitions between the valence and conduction bands.[1,2] The first two terms are negative and larger in absolute value than the third positive one, resulting in a negative diamagnetic susceptibility of $\chi_{dia}=-4.9\times10^{-7}$ emu/g Oe.[2] In contrast to bulk diamond, some all-carbon materials may show positive magnetization at 300 K, which can be associated with intrinsic paramagnetism or maybe even with ferromagnetism. Such magnetization behavior has been reported for several all-carbon materials including highly oriented pyrolitic graphite,[3,4] nanofoam,[5,6] nanodiamond,[7–10] and graphite nodules in a meteorite.[11] Esquinazi *et al.*[4] showed that magnetization of highly oriented pyrolitic graphite indicates very weak ferromagnetic properties with a Curie temperature above 300 K; proton irradiation of graphite results in more distinct ferromagneticlike magnetization.[12] Ohldag *et al.*[13] using soft x-ray dichroism experiments showed evidence that ferromagnetism observed in proton-irradiated metal-free carbon originates from the carbon π-electron system.

Nanodiamond,[14] a fascinating all-carbon nanomaterial, has become a subject of significant interest in the past several years. Data obtained by EPR[8–10] and NMR[9,10,15,16] show that nanodiamond may have predominant paramagnetic properties due to the presence of intrinsic paramagnetic centers. Talapatra *et al.*[17] reported that nanodiamond with implanted nitrogen shows enhanced ferromagnetic properties assigned to C–N bonding states. Thus, various experiments have indicated ferromagnetism of all-carbon materials including nanodiamond, but on balance, the question whether carbon can be ferromagnetic remains open. Although some theoretical models support the possibility of magnetic order in all-carbon nanomaterials,[18,19] the absence of iron-containing ferromagneticlike (ferro- or ferrimagnetic) phases, e.g., oxides, carbides, borides, or nitrides, needs to be carefully established before assigning the magnetic order to carbon.

High-resolution solid state NMR is a powerful method for studying diamagnetic materials, while its application to materials containing paramagnetic centers, i.e., paramagnetic ions, defects, or radicals with unpaired electrons, has been limited.[20] If paramagnetic centers are present in a material as a regular element of the lattice, they can strongly affect nuclear spin-spin and spin-lattice relaxation due to dipole-dipole coupling and Fermi hyperfine interaction, resulting in so-called paramagnetic effects. However, in magnetically heterogeneous materials where magnetic inclusions are present in the diamagnetic matrix as a separate phase, the effect of unpaired electrons located in these inclusions, i.e., extrinsic to the matrix, is not as strong as that of paramagnetic centers intrinsic to a material.[21–23] Hence, simultaneous studies of magnetic properties and NMR relaxation times of all-carbon materials can provide a better understanding of their magnetism. In this paper, we present a detailed study of the bulk magnetization and ^{13}C NMR relaxation data along

with a composition analysis of three different nanodiamond powder samples and discuss their magnetism.

II. EXPERIMENTAL DETAILS

Two samples of chemically purified nanodiamond powder, CAS No. 7782-40-3, of two different purities, ND-1 (97% purity) and ND-2 (95% purity), were obtained from Sigma-Aldrich. The third sample, ND-3, containing more impurities than ND-1 but less than ND-2, was obtained from A. Frishman (Iowa State University). Microdiamond was also purchased from Sigma-Aldrich. The nanodiamond grain size was estimated from peak widths in wide-angle x-ray powder diffraction using the Scherrer equation. The bulk magnetization of nanodiamond powder samples was measured at 1.8 and 300 K by a Quantum Design superconducting quantum interference device magnetometer in magnetic fields, H, varying between −70 and +70 kOe. For measurements, nanodiamond powder samples were placed in a gel capsule with a diamagnetic magnetic susceptibility of $\chi_{dia} = -1.3 \times 10^{-8}$ emu/g Oe, which is an order of magnitude smaller than the lowest magnetic susceptibility of nanodiamond powder. The uncertainties of the measurements were less than 2%.[21]

NMR experiments were performed at ambient temperature on a Bruker Biospin (Billerica, MA) DSX-400 spectrometer at a resonance frequency of 100 MHz for ^{13}C using a 7-mm Bruker magic angle spinning (MAS) probe. The 6.5-kHz MAS ^{13}C signal was detected from a sample packed into a 7-mm rotor. The ^{13}C $T_{1,C}$ relaxation time of nanodiamond was measured by the direct polarization T_1 method where the fully relaxed magnetization (after a recycle delay of 10 s) is stored alternately along the $+z$ and $-z$ directions. During the relaxation delay, which varied from 1 to 2000 ms, the magnetization effectively relaxed as e^{-t/T_1}. The ^{13}C $T_{1,C}$ relaxation time of microdiamond was determined by a saturation-recovery experiment with relaxation delays up to 2000 s.

The morphology and composition of nanodiamond powder samples were studied by two scanning electron microscopes (SEMs): a Hitachi S-2460N variable pressure SEM and JEOL JSM-840A SEM equipped with backscattered-electron and secondary electron detectors. Both SEMs also are equipped with energy-dispersive spectrometers (EDSs) for elemental analysis on a microscopic scale. The composition analysis was performed in a He environment at a pressure of 40 Pa because nanodiamond powder is not electrically conductive. The bulk composition of the samples was studied by a Phillips PW2404 x-ray fluorescence (XRF) spectrometer.

III. EXPERIMENTAL RESULTS

X-ray diffraction. Figure 1 shows wide-angle x-ray powder diffraction patterns of nanodiamond ND-1 and microdiamond. The Bragg peaks in the diffraction pattern of nanodiamond powder are much broader than those of microdiamond, indicating much smaller crystalline grain size. The size of

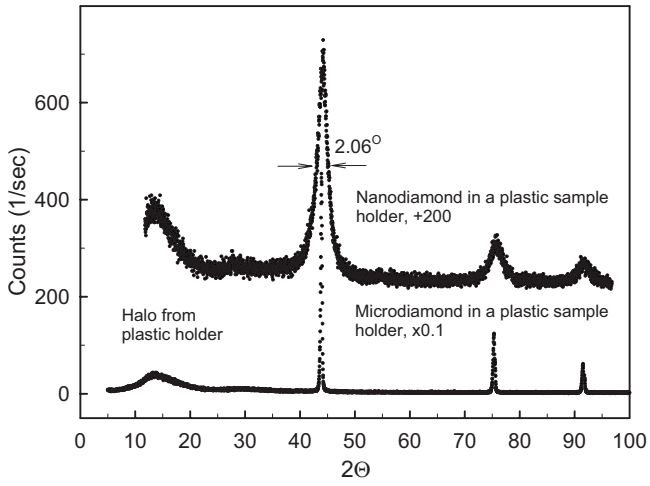

FIG. 1. Wide-angle x-ray diffraction pattern of nanodiamond powder ND-1. Data for microdiamonds are shown for reference.

crystalline grains was estimated by the Scherrer equation for spherical particles[24]

$$L = \frac{0.9\lambda}{\beta_{1/2} \cos \theta}, \tag{1}$$

where L is the crystal diameter, $\lambda = 0.154$ nm is the x-ray wavelength used, and $\beta_{1/2} = 2.06° = 0.0359$ rad is the full width in radians at half maximum intensity of the peak at $\theta = 22°$. The peak at 75° gives a similar size of nanodiamond grains within the uncertainty of measurements. Our data show that the average diameter of the crystalline core of the nanodiamond grains is 4.1 ± 0.2 nm, which agrees well with published data.[10,14]

Magnetic measurements. Figure 2 presents the magnetization of nanodiamond sample ND-1 measured at various temperatures. At 1.8 K, ND-1 has positive magnetization and shows a saturated magnetization of 1.2 emu/g in 55 kOe. At 300 K, ND-1 exhibits ferromagneticlike magnetization from 0 to ~0.01 emu/g when the magnetic field increases from 0 to ~2 kOe [see inset in Fig. 2(a)]. In higher magnetic fields, the value of the magnetization decreases and its sign inverts at ~20 kOe, showing that in high magnetic fields ND-1 has predominantly diamagnetic properties. A jump in the magnetization observed at ~20 kOe is due to a peculiarity of the magnetometer used, which shows large uncertainty of measurements during the signal sign inversion. The coercive force and remanent magnetization of ND-1 estimated from the magnetization data at 300 K are small, about 100 Oe and 0.001 emu/g, respectively. The M/H slope of ND-1 estimated from the plot at $H > 20$ kOe after subtraction of the contribution from the gel capsule is -3.4×10^{-7} emu/g Oe. Figure 2(b) shows the magnetization of ND-1 measured at 1.8, 5, 10, 20, and 30 K. The hysteresis of the magnetization of ND-1 measured at 1.8 K in magnetic fields varied between −70 and 70 kOe is only a few Oe, which is less than the uncertainty of magnetic measurements.

Figure 3 shows the magnetization of ND-2 and ND-3 samples measured at 1.8 and 300 K. The magnetization of

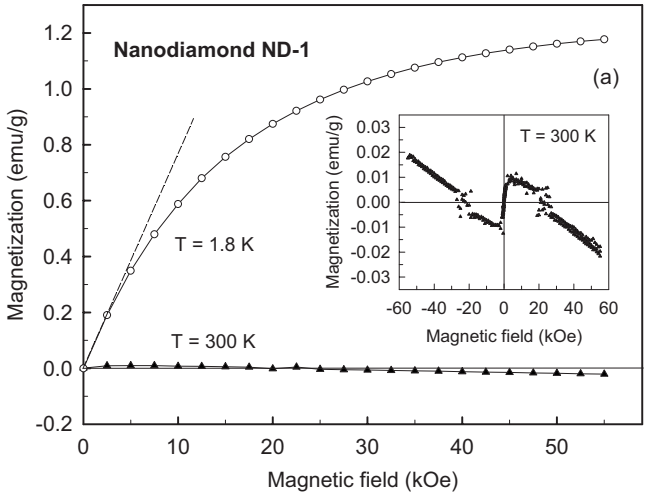

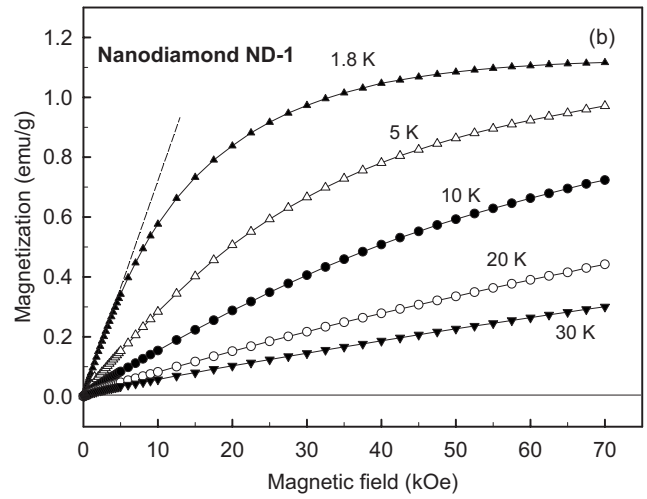

FIG. 2. Magnetization of nanodiamond ND-1 (15.6 mg sample mass) measured (a) at 1.8 and 300 K in magnetic fields from 0 to 55 kOe and (b) at 1.8, 5, 10, 20, and 30 K in magnetic fields from 0 to 70 kOe. The dashed lines show the initial magnetic susceptibility, $dM/dH|_0$. The inset in (a) shows an expanded view of the magnetization of ND-1 measured at 300 K for two directions of the magnetic field.

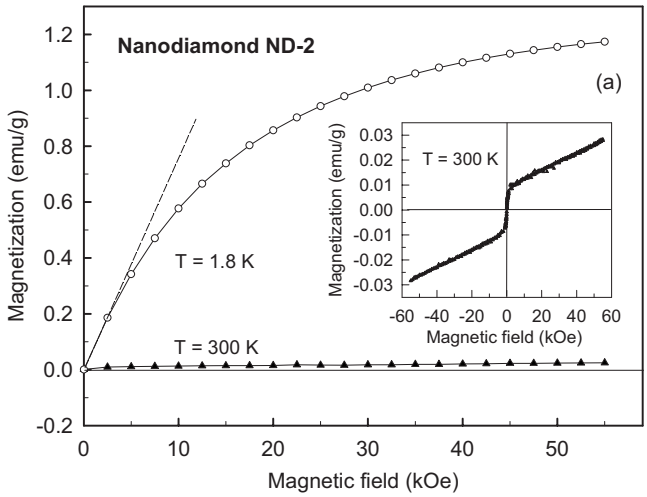

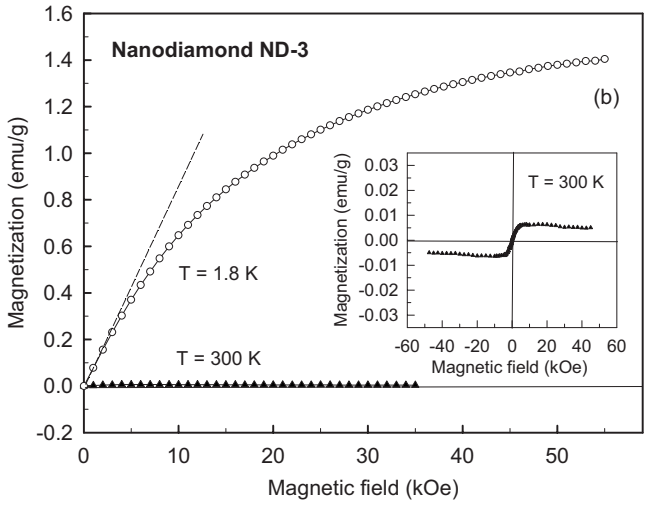

FIG. 3. Magnetization of nanodiamond samples (a) ND-2 (16.3 mg sample mass) and (b) ND-3 (24.8 mg sample mass) measured at 1.8 and 300 K. The insets show expanded views of the magnetization measured at 300 K for two directions of the magnetic field.

ND-2 at 1.8 K is very similar to that observed for ND-1, $\sim$1.2 emu/g in 55 kOe, while that measured at 300 K shows positive values in all magnetic fields used. ND-2 has ferromagneticlike magnetization when the magnetic field increases from 0 to $\sim$2 kOe and then increases linearly with a positive slope of 3.3×10^{-7} emu/g Oe. Hence, at 300 K, ND-2 in contrast to ND-1 has predominantly positive magnetization in all magnetic fields used. Magnetization of ND-3 at 1.8 K is similar to that observed for ND-1 and ND-2 but its saturation magnetization is slightly larger, 1.4 emu/g in 55 kOe. The initial magnetic susceptibility of ND-1 and ND-2 obtained at 1.8 K as the M/H ratio from the M vs H plots (see the dashed lines on Fig. 2) is similar, 7×10^{-5} emu/g Oe. M/H of ND-3 at 1.8 K, 7.8×10^{-5} emu/g Oe (Fig. 3) is also slightly larger than that of ND-1 and ND-2. At 300 K, the magnetization of ND-3 also first shows ferromagneticlike character but with slightly smaller $M_{fer}\approx0.008$ emu/g at $\sim$2 kOe and then decreases with a small negative slope of -0.4×10^{-7} emu/g Oe [see inset in Fig. 3(b)].

Figure 4 shows the temperature dependencies of the M/H ratio of ND-1 and ND-2 measured in various magnetic fields. The magnetic susceptibility obtained for ND-1 and ND-2, as well as ND-3 (not shown here) at 1.8 K from direct measurements in 10 kOe is very similar, 6.3×10^{-5} emu/g Oe. M/H of ND-1 measured in 40 kOe changes sign from positive to negative at $\sim$230 K, which agrees with the magnetization data [see inset in Fig. 2(a)]. The inset in Fig. 4(a) shows the temperature dependencies of the inverse ratio, H/M, for the same magnetic fields. Nonlinear H/M vs T dependencies when measured in 3 and 40 kOe can be explained by a combination of positive and negative temperature-independent contributions, respectively, while that measured in a 10 kOe

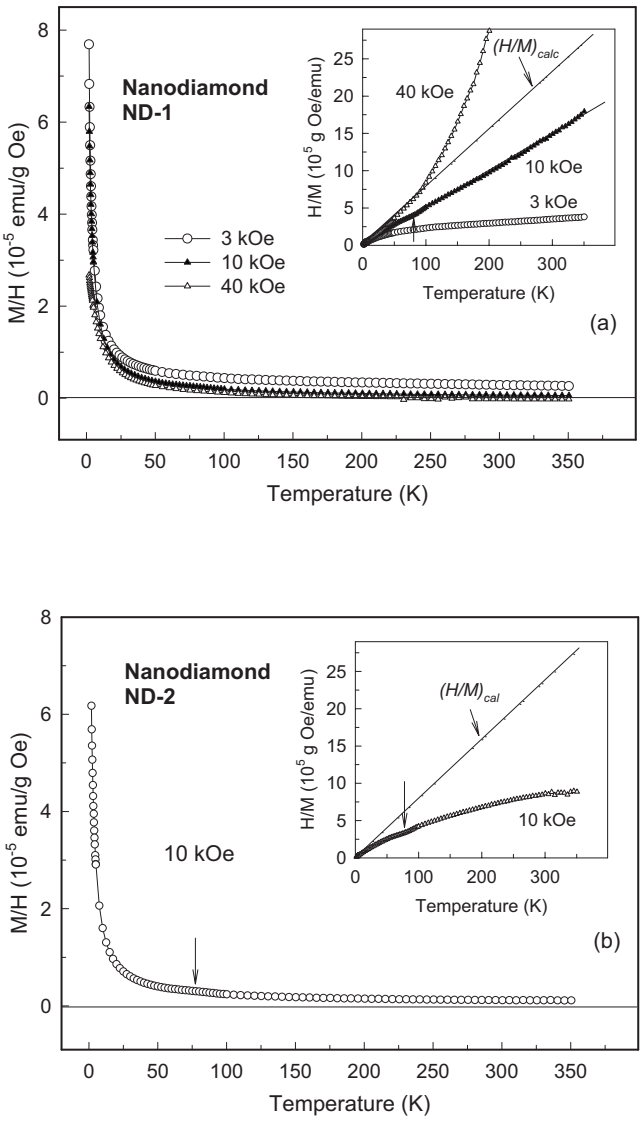

FIG. 4. Temperature dependencies of the M/H ratio of nanodiamond samples (a) ND-1 and (b) ND-2 measured in various magnetic fields. The insets show the experimental and calculated H/M ratios for the same samples. The anomalies in the magnetization of both samples are marked by vertical arrows.

magnetic field can be fitted by the Curie law showing that nearly constant positive (ferromagneticlike) and negative (diamagnetic) contributions cancel each other. The nonlinear increase of H/M of ND-2 measured in the same 10-kOe field can be explained by a larger positive temperature-independent contribution due to the presence of a larger amount of ferromagneticlike phase. The temperature dependencies of the $(H/M)_{calc}$ ratio of ND-1 and ND-2 samples shown in Figs. 4(a) and 4(b) as straight lines were calculated using the Curie law and the magnetic susceptibility of 7×10^{-5} emu/g Oe obtained for both samples as the M/H slope at 1.8 K. The M/H and H/M ratios of these samples measured in the 10 kOe field show an anomaly at ~80 K, which is indicated in Figs. 4(a) and 4(b) and both insets by vertical arrows; ND-2 has a slightly larger anomaly. The temperature dependence of the M/H ratio of ND-3 in the temperature range of 1.8–350 K (not shown here) is similar to that of ND-1 and ND-2. Hence, all three used samples show very similar magnetic properties at 1.8 K but different at 300 K (see Table I).

Figure 5 shows the magnetization of ND-1 and ND-2 measured under various conditions: cooled in zero or nonzero magnetic field and measured in zero or nonzero magnetic field. The magnetization of both samples cooled in zero field and at 10 kOe and measured in 10 kOe magnetic field shows quite similar behavior, while that cooled in 10 kOe and measured in zero magnetic field indicates insignificant remanent magnetization over a wide temperature range. Note that ND-1 cooled in 55 kOe and measured in 10 kOe shows quite similar magnetic susceptibility as that of zero magnetic field cooled sample. Thus, although some ferromagnetic phases are present in nanodiamond powder, the temperature dependencies of the magnetization of nanodiamonds at low temperatures are mostly determined by orientational paramagnetism.

Spatially resolved elemental analysis. To better understand the source of positive ferromagneticlike magnetization observed for nanodiamond powder samples, we have studied their morphology and composition on a microscopic scale. Figures 6(a) and 6(b) show ×1500 and ×50 000 backscattered-electron images of ND-1. The nanodiamond grains form clusters of larger size and then agglomerates of several microns diameter, which is consistent with the data by Dolmatov.[14] An overlay of energy-dispersive spectra of ND-1 [see Fig. 6(c)] obtained for the entire area of $90 \times 60\ \mu m^2$ [Fig. 6(a)] indicates that the total concentration of Fe does not exceed the background. Based on these data one might conclude that there is no Fe or, more correctly, that the concentration of Fe is below the detection limit of EDS (<0.1 mass %). In contrast, detailed composition analysis of bright spots shows that some of them contain a significant amount of Fe. A very similar situation was observed for

TABLE I. Fe content and magnetic parameters of nanodiamond samples at 1.8 and 300 K. The samples are listed according to their Fe content.

Sample	Fe content[a] (mass %)	M_{fer}, 300 K (emu/g)	M/H, 300 K, >2 kOe (emu/g Oe)	M, 1.8 K, 55 kOe (emu/g)	M/H, 1.8 K (emu/g Oe)
ND-1	0.3	0.01	-3.4×10^{-7}	1.2	7×10^{-5}
ND-3	0.4	0.008	-0.4×10^{-7}	1.4	7.8×10^{-5}
ND-2	0.6	0.01	3.3×10^{-7}	1.2	7×10^{-5}

[a]Obtained by x-ray fluorescence analysis.

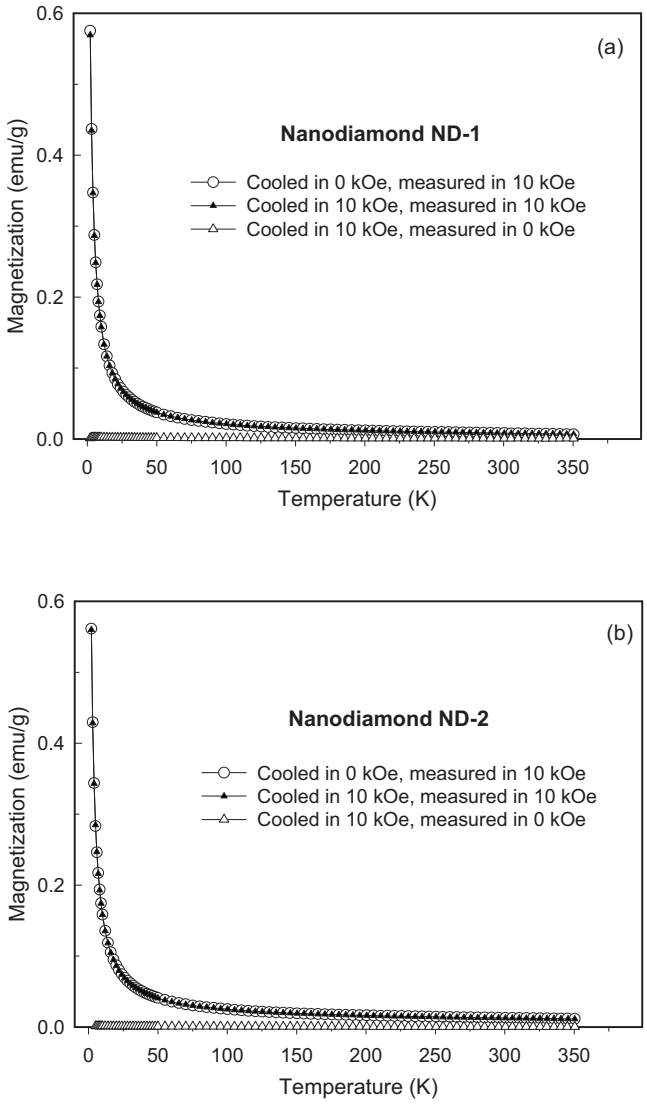

FIG. 5. Temperature dependencies of the magnetization of (a) ND-1 and (b) ND-2 measured under various conditions.

ND-2 and ND-3. Since EDS of nanoscale powder can be less than representative, all three nanodiamond powder samples were also studied by XRF; we found that ND-1, ND-3, and ND-2 nanodiamonds contain ~0.3, 0.4, and 0.6 mass % Fe, respectively.

^{13}C *NMR relaxation*. Figure 7 shows ^{13}C NMR spin-lattice, $T_{1,C}$, relaxation in nanodiamond powder ND-1 and synthetic and natural microdiamonds. The inset in Fig. 7 shows $T_{1,C}$ relaxation of the microdiamonds on a longer time scale. The relaxation in nanodiamond, $T_{1,C} \sim 0.2$ s, is more than 3 orders of magnitude faster than in synthetic, $T_{1,C} \sim 250$ s, and natural, $T_{1,C} \sim 750$ s, microdiamonds. This is strong evidence that $T_{1,C}$ relaxation in nanodiamond is reduced by an additional mechanism, which can be assigned to unpaired electrons in nanodiamond grains.

IV. PARAMAGNETISM AND FERROMAGNETISM OF NANODIAMOND POWDER

Contributions to the bulk magnetization. The magnetic field and temperature dependencies of M, M/H, and H/M of all nanodiamond samples at low temperatures can be assigned predominantly to orientational paramagnetism. Both the temperature and magnetic field dependences of the magnetization show the presence of several contributions. Nonlinear dependencies of the H/M ratio with a positive (measured in 3 kOe) and negative (measured in 40 kOe) curvature indicate that the paramagnetic and ferromagneticlike contributions arise from different phases. The slope of the magnetization of ND-1 at 300 K above ~20 kOe is negative, $M/H = -3.4 \times 10^{-7}$ emu/g Oe; that of ND-3 is also negative but of smaller magnitude, $M/H = -0.4 \times 10^{-7}$ emu/g Oe. The slope of the magnetization of ND-2 at 300 K above 2 kOe shows a dominant paramagnetic contribution, $M/H = 3.3 \times 10^{-7}$ emu/g Oe. The difference in slopes can be attributed to smaller paramagnetic contributions at 300 K in ND-3 than in ND-2 but larger than in ND-1 and is generally consistent with the Fe content (see Table I). Given that the paramagnetism at 1.8 K is nearly identical in the three samples, the different magnetization at 300 K above the saturation must be attributed to a superparamagnetic component associated with some of the Fe-containing inclusions in the sample. Hence, the total magnetization of nanodiamond powder samples measured in the experiments, M_{exp}, can be described as the sum of four contributions: negative diamagnetic, M_{dia}, positive paramagnetic, M_{par}, superparamagnetic, M_{sup}, and ferromagneticlike, M_{fer}.

Diamagnetic susceptibility. In the context of our data, it is interesting to note that Hudgens *et al.*[1] deduced a significant positive contribution to the total diamagnetic susceptibility, up to 55%, from virtual magnetic dipole transitions between the valence and conduction bands (Van Vleck paramagnetic term). Since the band structure may be affected by the small size of the diamond particles resulting in a reduction of the positive Van Vleck contribution, the magnetic susceptibility of nanodiamond could be somewhat more negative than that of bulk diamond. The estimation of the diamagnetic susceptibility of ND-1 based on the observed slope at 300 K in $H > 2$ kOe [-3.4×10^{-7} emu/g Oe, see inset in Fig. 2(a) and Table I], and calculated paramagnetic susceptibility ($\sim 4 \times 10^{-7}$ emu/g Oe) gives $\chi_{dia} \approx -7 \times 10^{-7}$ emu/g Oe, which is more negative than that of bulk diamond.

Ferromagneticlike behavior. The ferromagneticlike (ferro- or ferrimagnetic) contribution, M_{fer}, estimated from the saturation magnetization at 300 K for all three nanodiamond samples is very similar, ~0.01 emu/g (see Table I). This might suggest that ferromagnetism is an intrinsic property of nanodiamonds as proposed in Ref. 17. However, if the saturation magnetization of 0.01 emu/g is assigned to ferromagnetic order of spins with $S=1/2$, $L=0$, $J=S$, and $p_{eff} = 1\mu_B$,[25] located in each nanodiamond grain or particle, the concentration of such spins, called "ferromagnetic" spins in the following, should be about 4×10^{18} spins/cm^3. The average diameter of nanodiamond particles is ~4.6 nm (which includes a 0.25-nm thick noncrystalline shell around the 4.1-nm crystalline core[26]); this leads to a concentration of 2×10^{19} particles/cm^3. Hence, the average number of ferromagnetic spins per particle is expected to be less than one and, therefore, cannot result in magnetic order. The number of spins per grain will be smaller if $p_{eff} = g[S(S+1)]^{1/2} = 1.73\mu_B$,[25] for spins with $S=1/2$ is used in the calculations.

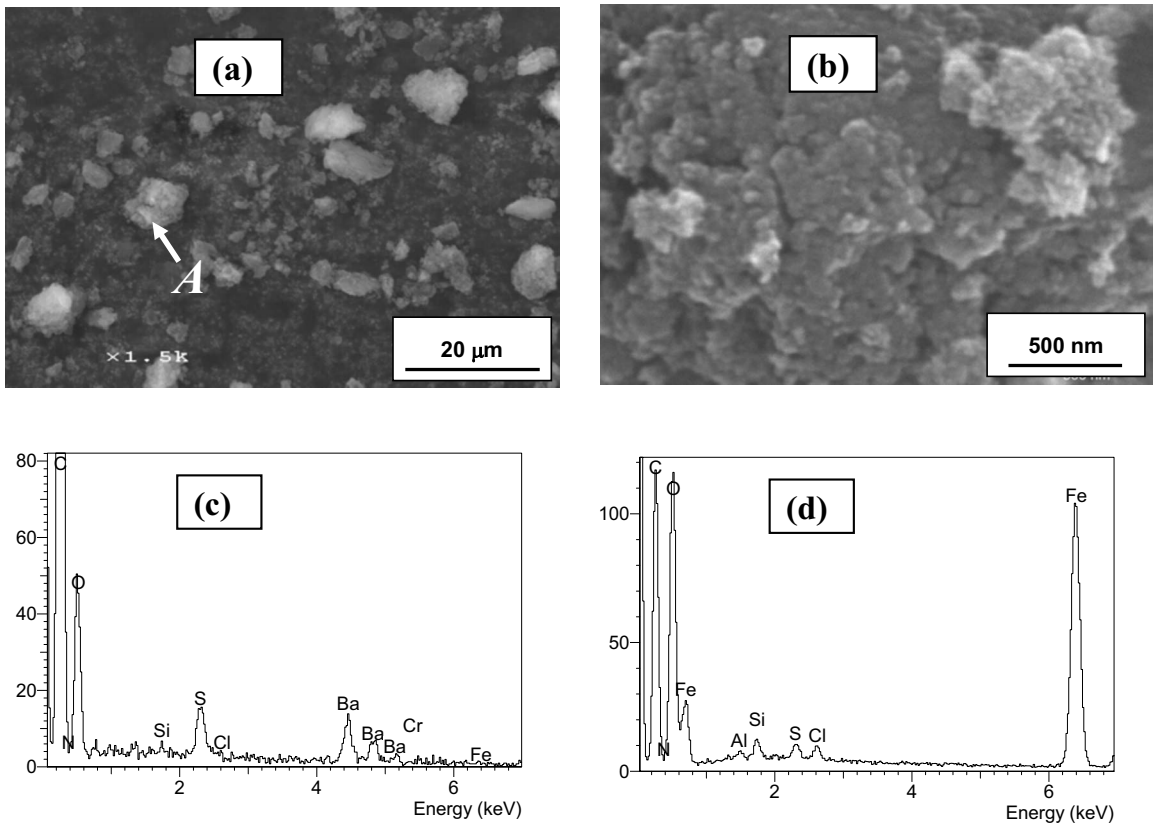

FIG. 6. Morphology and composition of nanodiamond ND-1: (a) SEM backscattered-electron image obtained at ×1500 and (b) ×50 000; note that large grains consist of agglomerated nanoparticles. (c) Composition obtained by energy-dispersive spectroscopy for the area shown in (a). (d) Composition of one of the iron-bearing grains marked by *A* in (a).

Furthermore, even if the concentration of ferromagnetic spins is larger than estimated and should result in ferromagnetic order in each grain, high-resolution NMR spectra would not be obtained due to expected strong dipolar and particularly hyperfine interactions[20] of ferromagnetic spins with carbon nuclei in the nanodiamond grain.

Hence, we must conclude that the ferromagneticlike behavior of the magnetization of nanodiamond is determined instead by a small amount of separate ferro- or ferrimagnetic phases, such as α-Fe_2O_3, γ-Fe_2O_3, Fe_3O_4, Fe_3C, Fe_2C, and/or Fe_4N, Fe_8N.[25,27] Talyzin *et al.*[28] recently showed that ferromagnetism of Rh-C_{60} is due to a separate phase, Fe_3C, and not to the carbon as originally reported in Ref. 29, which was retracted in Ref. 30. The value of the magnetization $M_{fer} \approx 0.01$ emu/g observed in ND-1 corresponds to ~0.012 mass % of γ-Fe_2O_3 and Fe_3O_4 (with saturation magnetization of 70–90 emu/g at 300 K) or 2.5 mass % of α-Fe_2O_3 (with saturation magnetization of 0.4 emu/g at 300 K),[27] if they are considered as the magnetically ordered phase present in nanodiamond powder. Hence, ferromagnetism should be considered as a "natural" property of nanodiamond powder obtained by the detonation method, but not of nanodiamond grains. From this point of view, ferromagnetism of nanodiamond and its enhancement after nitrogen implantation as reported in Ref. 17 can be understood by taking into consideration that nitrogen implantation can form ferromagnetic iron nitrides, which have a higher saturation moment than iron oxides and even pure iron.[25,31]

Paramagnetic behavior. The magnetization of nanodiamond at low temperatures is mostly determined by the paramagnetic component, particularly below ~30 K where the magnitude of M_{par} is significantly larger than M_{fer} and M_{dia}.

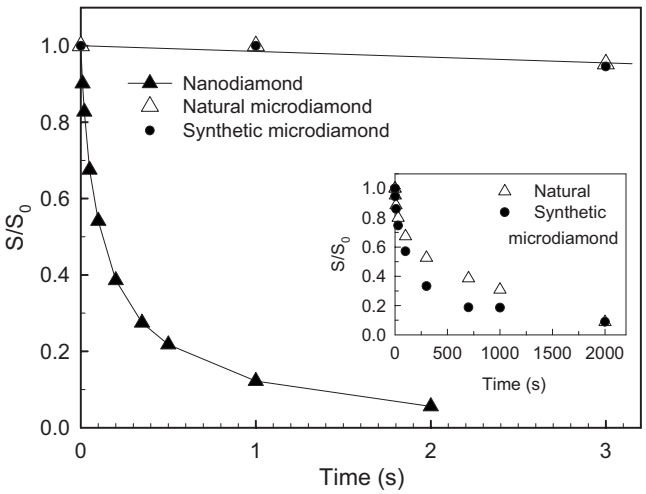

FIG. 7. ^{13}C NMR spin-lattice, $T_{1,C}$, relaxation of nanodiamond ND-1. Data for natural and synthetic microdiamonds are shown for reference; the inset presents an expanded view of their $T_{1,C}$ relaxation curves.

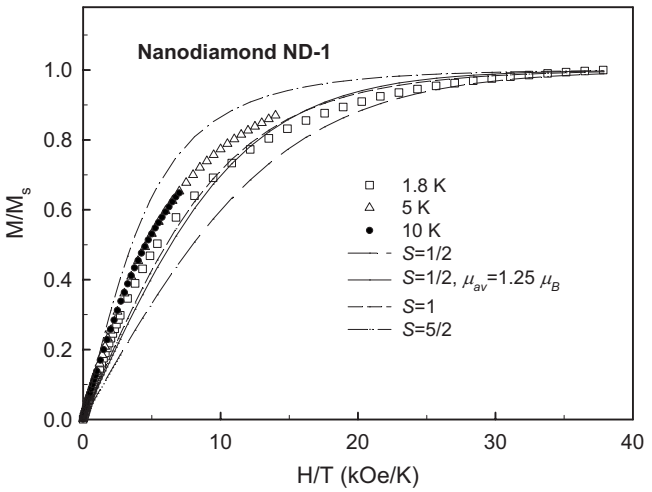

FIG. 8. Dependence of the M/M_s ratio vs H/T for ND-1, where M_s is the saturation magnetization, estimated from the experiment in the highest magnetic field. The magnetization, M, has been corrected for the diamagnetic contribution. The Brillouin functions for noninteracting 1/2, 1, and 5/2 spins are shown by long-dashed, short-dashed, and dash-dotted lines, respectively. The curve for $S=1/2$ with the average magnetic moment of $\mu_{av}=1.25\mu_B$ is shown by a continuous line.

Note that the highest purity of nanodiamond typically is obtained by chemical treatment,[9,10,14] which reduces the concentration of Fe-bearing inclusions. However, the M/H ratio of all three samples measured at 1.8 K in 10 kOe is very similar, 6.3×10^{-5} emu/g Oe. The bulk magnetization of all nanodiamond samples studied at 1.8 K also is very similar, 1.3 ± 0.1 emu/g, showing that low-temperature paramagnetism does not depend on the Fe content (see Table I). Therefore, we conclude that the observed magnetization curves at 1.8 K should be associated mostly with the paramagnetic centers intrinsic to nanodiamond.

The magnetic field dependence of the magnetization of noninteracting paramagnetic ions with spins S can be described by the Brillouin function $B_S(y)$ (Refs. 25 and 32)

$$B_S(y)=\frac{2S+1}{2S}\coth\left(\frac{2S+1}{2S}y\right)-\frac{1}{2S}\coth\left(\frac{1}{2S}y\right) \qquad (2)$$

with $y=Sx$ and $x=g\mu_BH/kT$, where g is the Lande factor. For $S=1/2$ or $S=\infty$ the Brillouin function transforms to the hyperbolic tangent $B_{1/2}[(1/2)x]=\tanh[(1/2)x]$ or the Langevin function $L(x)=\coth(x)-1/x$, respectively.[32] Figure 8 exhibits the dependence of the M/M_s ratio of ND-1 vs H/T plotted on the basis of the experimental data shown in Fig. 2(b). At 1.8 K, this dependence can be satisfactorily fitted by the Brillouin function for spins $S=1/2$ if the average magnetic moment used is $\mu_{av}=1.25\mu_B$, or for spins $S=1$. Note that the magnetization of nanofoam was satisfactory fitted by the Langevin function if the average magnetic moment used is $12.5\mu_B$, which was taken to suggest a clustering of the $S=1/2$ spins.[6] The Brillouin function for spins $S=5/2$ does not fit the dependence of the M/M_s ratio of ND-1 vs H/T. Hence, our data indicate that paramagnetism of nanodiamond powder at low temperature can be associated with electron spins of $S=1/2$ or 1. Note that $S=1$ seems unlikely since EPR spectra of Shames *et al.*[9,10] do not show any indication of the (first-order forbidden) $|\Delta m|=2$ transition characteristic of a spin-1 state.

The magnetization of all studied nanodiamonds at 300 K in contrast to 1.8 K is quite different showing a large change in the M/H slope [see insets in Figs. 2(a), 3(a), and 3(b) and Table I]. If the positive slope of $\chi_{exp}=3.3\times10^{-7}$ emu/g Oe observed for ND-2 at 300 K in magnetic fields >20 kOe is associated with the paramagnetism, then $\chi_{par}=\chi_{exp}+|\chi_{dia}|=8.2\times10^{-7}$ emu/g Oe, where we used $|\chi_{dia}|=|-4.9\times10^{-7}|$ emu/g Oe.[2] Extrapolating this paramagnetic contribution to 1.8 K using the Curie law gives 14×10^{-5} emu/g Oe, which is twice larger than the magnetic susceptibility measured at 1.8 K. If the diamagnetic susceptibility of $\chi_{dia}\approx-7\times10^{-7}$ emu/g Oe, suggested for nanodiamond (see above), should be used instead of that of bulk diamond, the extrapolated paramagnetic susceptibility at 1.8 K would be even larger. Such a behavior of the magnetization requires us to suggest that ND-3 and particularly ND-2 contain an additional positive paramagnetic contribution. The M/H slope, i.e., the magnitude of the contribution, well correlates with the Fe content (Table I) showing that it can be from single-domain magnetically ordered small inclusions with superparamagnetic properties.[33] Such a contribution can be significant at high but not at low temperatures due to its decrease below the "blocking temperature," T_b. Some features observed by us at ~80 K (see Fig. 4) and by Osipov *et al.*[34] can be associated with T_b in superparamagnetic system. On the other hand, we cannot exclude that the anomaly at ~80 K is due to the presence of paramagnetic oxygen as was suggested in Ref. 34.

Electron spin concentration. At 300 K, M_{fer} saturates in ~2 kOe while the magnitude of M_{par} and M_{dia} changes linearly with the magnetic field and in $H\geq40$ kOe M_{fer} is negligible compared to M_{par} and M_{dia}. Furthermore, M_{dia} is temperature independent and M_{fer} of iron oxides is nearly temperature independent, while M_{par} changes as $1/T$. Note that M_{fer} and M_{dia} can cancel each other in a certain magnetic field as observed for ND-1 in 10 kOe. Hence, the temperature dependence of M/H of ND-1 measured in 10 kOe represents mostly the paramagnetic contribution, M_{par}/H, and can be fitted by the Curie law

$$M_{par}/H=\chi_{par}=(Np_{eff}^2)/3kT=C/T, \qquad (3)$$

where χ_{par} is the magnetic susceptibility measured experimentally, N is the Avogadro number, k is the Boltzmann constant, p_{eff} is the effective magnetic moment, and C is the Curie constant.[25] Thus, the temperature dependence of the magnetization of nanodiamond at low temperatures can be associated mostly with orientational paramagnetism and the best value of the paramagnetic contribution can be obtained from our data at 1.8 K. Using $\chi_{par}=7\times10^{-5}$ emu/g Oe, obtained at 1.8 K as the initial slope of $M(H)$, we calculated C and then from the $(M/H)_{cal}\sim C/T$ dependence [see $(H/M)_{cal}$ dependence in the insets in Figs. 4(a) and 4(b)], we obtained $\chi_{par}\approx4\times10^{-7}$ emu/g Oe at 300 K. This value is suitable for estimating the concentration of unpaired electrons in nano-

TABLE II. Spin concentration in nanodiamond and nanofoam.

Sample	Spin concentration (spins/g)	Obtained from	Reference
Nanodiamond	2.4×10^{20}	1.8 K magnetic susceptibility data	This work
	0.96×10^{20}	Curie constant	7
	0.42×10^{20}	1.9 K magnetization data	10
	$\sim10^{20}$	EPR	8 and 9
Nanofoam	1.8×10^{20}	EPR	5

diamond. The number of spins per gram of substance, N_s, can be found as

$$N_s = (\chi_{par} 3kT)/(p_{eff}^2), \tag{4}$$

where $p_{eff}=1.73\mu_B$ for $L=0$, $J=S$ corresponds to the effective magnetic moment of one unpaired electron ($S=1/2$) and $1\mu_B=9.27\times10^{-21}$ erg/Oe.[25] The concentration of spins per gram estimated from the magnetic susceptibility of ND-1 by Eq. (4) is 2.4×10^{20} spins/g, which is approximately two- and fivefold higher than the values reported by Prasad *et al.*,[7] 0.96×10^{20} spins/g, and Shames *et al.*,[10] 0.42×10^{20} spins/g, respectively (see Table II).

All three values of spin concentration were calculated based on magnetization data: Prasad *et al.*[7] used the Curie constant obtained from the temperature dependence (2–300 K) of the magnetization, Shames *et al.*[10] used 1.9 K magnetization data, and we used data obtained at 1.8 K (where the contribution from the paramagnetic phase is the most dominant). The lowest spin concentration in nanodiamond is reported in Ref. 10; however, according to these data,[10] the magnetization of nanodiamond at 1.9 K in 50 kOe after the subtraction of the diamagnetic contribution is 0.35 emu/g, which is approximately threefold (not fivefold as the reported spin concentration) smaller than that measured in our experiments (see Table I). Such a difference in both the bulk magnetization and calculated spin concentration could be due to various reasons, e.g., different values of the density of the nanopowder samples, 3.52 and 2.62 g/cm^3 in Ref. 10 and our experiment, respectively. Note also that in Ref. 9, Shames *et al.* showed a higher spin concentration in nanodiamond, i.e., up to $\sim10^{20}$ spins/g based on the EPR data. The volume concentration of nanodiamond particles is 2×10^{19} particles/cm^3; hence, the spin concentration of 2.4×10^{20} spins/g obtained from our 1.8 K magnetic susceptibility and associated with the electron spins in nanodiamond grains corresponds to ~30 unpaired electrons per ~4.6 nm diameter nanodiamond grain on average. Because ND-2 and ND-3 show very similar bulk mass magnetization at 1.8 K to that of ND-1, we can conclude that they have similar concentrations of unpaired electrons.

Effect of unpaired electrons on NMR. NMR spectra reflect the effect of the environment on the nuclei, i.e., they show local properties of a material. Unpaired electrons of paramagnetic centers as a source of additional magnetic fields can affect NMR spectra via electron-nucleus dipole-dipole and Fermi interactions and significantly decrease nuclear spin relaxation times.[20] The effect of unpaired electrons on NMR spectra strongly depends on their distance to the nuclei, and also on transfer of electron density, resulting in a different effect from unpaired electrons intrinsic and extrinsic to the phases giving the NMR signal. NMR spectra of a paramagnetic single-phase substance can be obtained if its magnetic susceptibility is smaller than 2.2×10^{-6} emu/g Oe,[35] which in 94 kOe results in a magnetization of 0.2 emu/g. The paramagnetic susceptibility of 4×10^{-7} emu/g Oe measured for ND-1 at 300 K corresponds to a magnetization of 0.037 emu/g in 94 kOe, which is significantly smaller than the limit of NMR observability. Hence, this magnetization is too small to produce strong paramagnetic effects if the electron spins are located in a separate magnetic phase, but enough to decrease nuclear spin relaxation times if the electron spins are present in the same phase. This conclusion can be confirmed by our data for a model system, laponite mixed with Fe_2O_3 nanoparticles,[21–23] which showed that the effect of a separate ferromagnetic phase producing a bulk magnetization of ~0.04 emu/g on NMR spectra is insignificant. Hence, high-resolution NMR along with the measurement of the temperature and magnetic field dependencies of the magnetization can be used to distinguish intrinsic and extrinsic magnetism in all-carbon magnetic materials. Our detailed studies of nanodiamond powders by ^{13}C MAS NMR spectroscopy will be presented elsewhere.

The effect of unpaired electrons on the spin-lattice relaxation of carbon nuclei, $T_{1,C}$, depends on the distance r between the unpaired electron and the nucleus as $T_{1,C}\sim r^6$. The fast spin-lattice relaxation in nanodiamond powder (Fig. 7) is evidence that unpaired electrons are located inside the nanodiamond grains. Note that similarly fast $T_{1,C}$ relaxation for nanodiamond was recently observed by Panich *et al.*[16] Hence, our magnetization, NMR, and spatially resolved energy-dispersive spectroscopy data of nanodiamond powder suggest the presence of four contributions: (1) diamagnetic from carbon, (2) paramagnetic from unpaired electrons in nanodiamond grains, and (3) ferromagneticlike and (4) superparamagnetic contributions from Fe-containing particles.

Our data show that the measurements of the magnetization only at constant temperature (see, for example, Ref. 17) are not enough for elucidating the origin of the magnetism of all-carbon materials. We have demonstrated that ^{13}C NMR spectroscopy and relaxation-time measurements along with the measurements of the temperature and magnetic field dependencies of the magnetization can be used to distinguish effects of electron spins that are intrinsic or extrinsic to various all-carbon magnetic materials.

Likely origin of unpaired electrons in nanodiamond grains. The unpaired electrons in nanodiamond may arise from single substitutional N- or from C-related defects, which may result from vacancies located within the core or near the surface.[14,36–38] The defects due to single substitutional N, which are clearly identified by the triplet hyperfine structure arising from the $2I+1$ spin orientations of the $I=1$ nuclear spin of ^{14}N (see Ref. 38), are not observed in nanodiamond.[9,10] Also, according to Ref. 39, no N-related paramagnetic centers were detected in nanodiamond obtained by the detonation method. Hence, the unpaired electrons in nanodiamond must be attributed to C-related lattice defects.

Rode *et al.*[5] reported that carbon nanofoam produced by laser ablation shows paramagnetic and, possibly, ferromagnetic behavior. The saturation magnetization of nanofoam, $\sim 0.4-0.8$ emu/g measured at 1.8 K in 70 kOe, and the number of unpaired electrons obtained by EPR at low temperature, 1.8×10^{20} spins/g, are similar to those observed for nanodiamond. Recently, Arčon *et al.*[6] suggested that paramagnetism of nanofoam comes from sample regions with a curved layer structure and also from sp^3-like region. However, it is very likely that the coercive force of 420 Oe observed for nanofoam at 1.8 K (Ref. 5) is due to a ferromagneticlike Fe-containing phase present according to Ref. 6 in the nanofoam samples. Hence, the origin of magnetism in all-carbon materials still needs to be clarified depending on the type of a material and we cannot exclude categorically that similar behavior of the bulk magnetization of various all-carbon nanomaterials may have a different origin.

V. CONCLUSIONS

We have shown that the total magnetization of nanodiamond consists of contributions from (1) the diamagnetic effect of carbon, (2) the paramagnetic effect of unpaired electrons present in nanodiamond grains, and (3) ferromagneticlike and (4) superparamagnetic Fe-containing particles. Contributions (1) and (2) are intrinsic to nanodiamond, being observed similarly in three samples of different purity, while contributions (3) and (4) arise from small grains of iron-bearing phase(s) proven by spatially resolved energy-dispersive spectroscopy and retained in detonation nanodiamond even after chemical purification. A reduction of the $T_{1,C}$ relaxation time in ^{13}C NMR by 3 orders of magnitude in nanodiamond compared to natural and synthetic microdiamonds confirms the presence of unpaired electrons in nanodiamond grains, given that $T_{1,C}$ should be unaffected by the presence of the ferromagnetic particles with a bulk magnetization of ~ 0.01 emu/g at 300 K. The paramagnetic spin concentration corresponds to ~ 30 unpaired electrons per ~ 4.6 nm diameter nanodiamond grain. Our study demonstrates that NMR relaxation data along with detailed measurements of the temperature and magnetic field dependencies of the magnetization can be used to determine whether electron spins are intrinsic or extrinsic to all-carbon magnetic materials.

ACKNOWLEDGMENTS

E.M.L. and S.L.B. thank P. C. Canfield (Iowa State University) for his support of this work. Work at the Ames Laboratory was funded by the Department of Energy-Basic Energy Sciences under Contract No. DE-AC02-07CH11358.

*Corresponding authors: levin@iastate.edu or srohr@iastate.edu

[1] S. Hudgens, M. Kastner, and H. Fritzsche, Phys. Rev. Lett. **33**, 1552 (1974).
[2] J. Heremans, C. H. Olk, and D. T. Morelli, Phys. Rev. B **49**, 15122 (1994).
[3] R. Höhne and P. Esquinazi, Adv. Mater. (Weinheim, Ger.) **14**, 753 (2002).
[4] P. Esquinazi, A. Setzer, R. Höhne, C. Semmelhack, Y. Kopelevich, D. Spemann, T. Butz, B. Kohlstrunk, and M. Lösche, Phys. Rev. B **66**, 024429 (2002).
[5] A. V. Rode, E. G. Gamaly, A. G. Christy, J. F. Gerald, S. T. Hyde, R. G. Elliman, B. Luther-Davies, A. I. Veinger, J. Androulakis, and J. Giapintzakis, J. Magn. Magn. Mater. **290-291**, 298 (2005).
[6] D. Arčon, Z. Jagličič, A. Zorko, A. V. Rode, A. G. Christy, N. R. Madsen, E. G. Gamaly, and B. Luther-Davies, Phys. Rev. B **74**, 014438 (2006).
[7] B. L. V. Prasad, H. Sato, T. Enoki, Y. Hishiyama, Y. Kaburagi, A. M. Rao, P. C. Eklund, K. Oshida, and M. Endo, Phys. Rev. B **62**, 11209 (2000).
[8] P. I. Belobrov, S. K. Gordeev, E. A. Petrakovskaya, and O. V. Falaleev, Dokl. Phys. **46**, 459 (2001).
[9] A. I. Shames, A. M. Panich, W. Kempiński, A. E. Alexenskii, M. V. Baidakova, A. T. Dideikin, V. Yu. Osipov, V. I. Siklitski, E. Osawa, M. Ozawa, and A. Ya. Vul', J. Phys. Chem. Solids **63**, 1993 (2002).
[10] A. I. Shames, A. M. Panich, W. Kempiński, M. V. Baidakova, V. Yu. Osipov, T. Enoki, and A. Ya. Vul', in *Synthesis, Properties and Applications of Ultracrystalline Diamond*, NATO Series (Springer, New York, 2005), pp. 271–282.
[11] J. M. D. Coey, M. Venkatesan, C. B. Fitzgerald, A. P. Douvalis, and I. S. Sanders, Nature (London) **420**, 156 (2002).
[12] P. Esquinazi, D. Spemann, R. Höhne, A. Setzer, K.-H. Han, and T. Butz, Phys. Rev. Lett. **91**, 227201 (2003).
[13] H. Ohldag, T. Tyliszczak, R. Höhne, D. Spemann, P. Esquinazi, M. Ungureanu, and T. Butz, Phys. Rev. Lett. **98**, 187204 (2007).
[14] V. Yu. Dolmatov, Russ. Chem. Rev. **70**, 607 (2001).
[15] T. M. Alam, Mater. Chem. Phys. **85**, 310 (2004).
[16] A. M. Panich, A. I. Shames, H.-M. Vieth, E. Osawa, M. Takahashi, and A. Ya. Vul', Eur. Phys. J. B **52**, 397 (2006).
[17] S. Talapatra, P. G. Ganesan, T. Kim, R. Vajtai, M. Huang, M. Shima, G. Ramanath, D. Srivastava, S. C. Deevi, and P. M. Ajayan, Phys. Rev. Lett. **95**, 097201 (2005).
[18] N. Park, M. Yoon, S. Berber, J. Ihm, E. Osawa, and D. Tománek, Phys. Rev. Lett. **91**, 237204 (2003).
[19] H. Kumazaki and D. S. Hirashima, J. Phys. Soc. Jpn. **76**, 064713 (2007).
[20] I. Bertini and C. Luchinat, Coord. Chem. Rev. **150**, 1 (1996).

[21] E. M. Levin, S. S. Hou, S. L. Bud'ko, and K. Schmidt-Rohr, J. Appl. Phys. **96**, 5085 (2004).
[22] E. M. Levin, A. Rawal, S. L. Bud'ko, A. Kracher, and K. Schmidt-Rohr, J. Appl. Phys. **98**, 114315 (2005).
[23] E. M. Levin, S. L. Bud'ko, J. D. Mao, Y. Huang, and K. Schmidt-Rohr, Solid State Nucl. Magn. Reson. **31**, 63 (2007).
[24] H. P. Klug and L. E. Alexander, *X-Ray Diffraction Procedures*, 2nd ed. (Wiley, New York, 1974).
[25] S. Chikazumi, *Physics of Ferromagnetism*, 2nd ed. (Oxford Science, New York, 1997).
[26] K. Schmidt-Rohr, A. Rawal, and X.-W. Fang, J. Chem. Phys. **126**, 054701 (2007).
[27] B. M. Moskowitz, http://www.geo.umn.edu/orgs/irm/hg2m/hg2m_index.html
[28] A. Talyzin, A. Dzwilewski, L. Dubrovinsky, A. Setzer, and P. Esquinazi, Eur. Phys. J. B **55**, 57 (2007).
[29] T. L. Makarova, B. Sundqvist, R. Höhne, P. Esquinazi, Y. Kopelevich, P. Scharff, V. A. Davydov, L. S. Kashevarova, and A. V. Rakhmanina, Nature (London) **413**, 716 (2001).
[30] T. L. Makarova, B. Sundqvist, R. Höhne, P. Esquinazi, Y. Kopelevich, P. Scharff, V. A. Davydov, L. S. Kashevarova, and A. V. Rakhmanina, Nature (London) **440**, 707 (2006).
[31] S. F. Matar, J. Alloys Compd. **345**, 72 (2002).
[32] H. E. Staley, *Introduction to Phase Transitions and Critical Phenomena* (Clarendon, Oxford, 1971).
[33] E. P. Wohlfarth, J. Magn. Magn. Mater. **39**, 39 (1983).
[34] Yu. Osipov, T. Enoki, K. Takai, K. Takahara, M. Endo, T. Hayashi, Y. Hishiyama, Y. Kaburagi, and A. Ya. Vul', Carbon **44**, 1225 (2006).
[35] A. P. S. Mandair, P. J. Michael, and W. R. McWhinnie, Polyhedron **9**, 517 (1990).
[36] A. S. Barnard and M. Sternberg, J. Phys. Chem. B **109**, 17107 (2005).
[37] F. Jelezko and J. Wrachtrup, Phys. Status Solidi A **203**, 3207 (2006).
[38] A. Banaszak, K. Fabisiak, M. Kaczmarski, and M. Kozanecki, Cryst. Res. Technol. **41**, 535 (2006).
[39] K. Iakoubovskii, M. V. Baidakova, B. H. Wouters, A. Stesmans, G. J. Adriaenssens, A. Ya. Vul', and P. J. Grobet, Diamond Relat. Mater. **9**, 861 (2000).